Tobias Jurek*, Heiner Kuhlmann, and Christoph Holst

# Impact of spatial correlations on the surface estimation based on terrestrial laser scanning

https://doi.org/10.1515/jag-2017-0006
Received January 31, 2017; accepted June 1, 2017

**Abstract:** In terms of high precision requested deformation analyses, evaluating laser scan data requires the exact knowledge of the functional and stochastic model. If this is not given, a parameter estimation leads to insufficient results. Simulating a laser scanning scene provides the knowledge of the exact functional model of the surface. Thus, it is possible to investigate the impact of neglecting spatial correlations in the stochastic model. Here, this impact is quantified through statistical analysis.

The correlation function, the number of scanning points and the ratio of colored noise in the measurements determine the covariances in the simulated observations. It is shown that even for short correlation lengths of less than 10 cm and a low ratio of colored noise the global test as well as the parameter test are rejected. This indicates a bias and inconsistency in the parameter estimation. These results are transferable to similar tasks of laser scanner based surface approximation.

**Keywords:** terrestrial laser scanner, deformation analysis, spatial correlation, stochastic model

## 1 Motivation

Using terrestrial laser scanners (TLS) to acquire geometric properties of surfaces has been proven to be a solid procedure in tasks of industrial and classical survey [7, 10]. New TLS measure with a rate of up to one million points per second and generate a highly dense three-dimensional point cloud with a 3D point accuracy of a few millimeters [17]. Accordingly, they have a high spatiotemporal resolution.

This leads to the advantage of quick scanning, completely capturing the whole visible surface with no need of marked points. Hence, this instrument is especially useful to acquire the geometry of large or rather inaccessible areas, such as dams [20] or other buildings [2, 14]. If measured in several epochs, also changes of these geometries can, thus, be detected. This procedure leads to laser scanner based deformation analyses which are currently in focus of engineering geodesy [6].

A deformation analysis has to decide whether a deformation between two surfaces exists or not [27], i.e., if the difference between a measured point cloud and a reference is significant. The result of this decision depends on the stochastic characteristics of the point cloud. They are defined by the covariance matrix of the observations which consists of variances and covariances. Usually, the variances are approximately known from a-priori information or empirical investigations [12]. Yet, the correlations and, thus, the covariances are unknown and therefore neglected [3]. Determining the stochastic model is complex and there is no common approach to detect the unknown correlations in the observations yet [6].

Figure 1 shows the systematic residuals that occur when simulating the scan of a plane of $0.5 \times 0.5$ m in 10 m distance with existing correlations between the scan points. Due to these systematic structures, correlations have a formative effect on laser scans. The residuals of points which lie near to each other have similar magnitudes and signs. By showing four different realizations of the same stochastic process, the random component of correlation gets obvious. If this stochastic process and the underlying correlations are completely unknown, a deformation analysis can most probably not distinguish between systematic measurement errors and areal deformations.

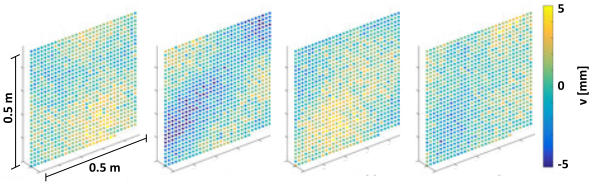


**Figure 1:** Different realizations of correlated observations and their residuals $v$.

The simulation will be explained in detail later on.

As consequence for a least-squares adjustment based on these observations degraded by unknown correlations, the parameter estimates may be inaccurate on the one

***Corresponding author: Tobias Jurek,** Institute of Geodesy and Geoinformation, University of Bonn, Nussallee 17, 53115, Bonn, Germany, e-mail: jurek@igg.uni-bonn.de
**Heiner Kuhlmann, Christoph Holst,** Institute of Geodesy and Geoinformation, University of Bonn, Nussallee 17, 53115, Bonn, Germany, e-mails: heiner.kuhlmann@uni-bonn.de, c.holst@igg.uni-bonn.de

hand. On the other hand, the corresponding standard deviations may be too optimistic or pessimistic, depending on the sign of the correlations [6]. Hence, due to the neglect of correlations, the parameter estimation may be biased and inconsistent. Both effects will be analyzed based on statistical tests in this paper.

Consequently, the significance of parameter changes at deformation analyses cannot be judged straightforward since the corresponding global test of the adjustment relies on a realistic stochastic model. Instead, most laser scanner based deformation analyses proof the object's deformation by assessing the parameters' accuracy empirically or based on experience (e.g., [5]).

Only few investigations have been published covering this issue but do not provide final solutions (Section 2.2). Therefore, this paper investigates the difference of knowing correlations in a parameter estimation compared to neglecting those in a simulated laser scan of a plane. In this way, it is possible to investigate and quantify effects of various factors in the process of a parameter estimation. This procedure is similar to a geodetic sensitivity analysis following Schwieger (2005) [34]: By varying selected input variables (here: correlations), the response of the output variables (here: estimated parameters and their covariance matrix) is studied using sensitivity values (here: global test, parameter test).

The paper is structured as follows: Section 2 illustrates the causes of correlations in TLS to provide a physical and mathematical basis. The process of generating correlated observations in a simulation environment is described in Section 3. The evaluation of the results is presented in Sections 4 and 5. The acquired results are discussed in Section 6, followed by the conclusion and outlook in Section 7.

# 2 Basics of correlations in laser scans

The present section describes the physical causes of correlations in laser scans (Section 2.1). Furthermore, Section 2.3 shows how they are mathematically integrated in the stochastic model of the observations. Studies regarding correlations in TLS are presented in Section 2.2. Thus, this section defines the basis for handling correlations in a parameter estimation.

## 2.1 Causes of correlations in laser scans

In most cases, measurements are handled as uncorrelated and, thus, stochastic independent. This does not reflect

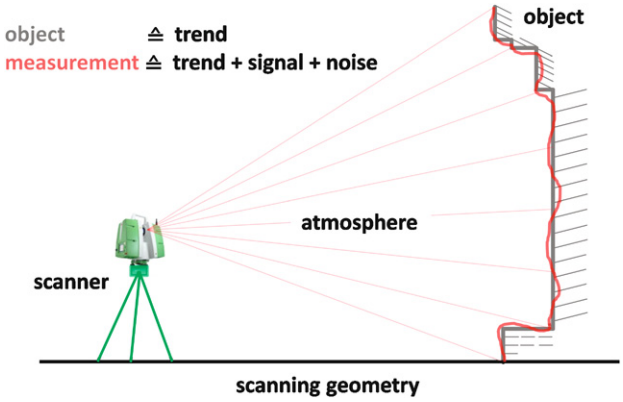


**Figure 2:** The three components of the measurements: trend, signal and noise. The trend is defined by the surface of the object. The signal includes correlating effects, caused by various influences.

the reality due to systematic effects which influence the uncertainties of multiple points in a similar way. All effects causing variances and covariances are generally distinguished as [31]:

- Scanner mechanism (calibration, settings),
- Atmospheric conditions (temperature, pressure),
- Object properties (color, reflection),
- Scanning geometry (incidence angle).

The scanner mechanism comprises the instrument's mechanical inaccuracies as well as the scanning settings. Considering minor changes in the manufacture and time-conditioned deterioration, laser scanners have to be calibrated [11]. Since the accuracy in the estimation of calibration parameters is limited, there are remaining fractions which cannot be determined by the calibration approach. Those are affecting the observations systematically [7], leading to similar systematic errors of neighbored points. Furthermore, the instrument's warm up process and interval of usage cause slight changes in the measuring units due to the operating temperature [17], which changes in time.

In terms of scanning settings, different measuring options like the resolution or quality levels [17] lead to varying correlations between the distance measurements of neighbored points. Consequently, effects related to the scanner mechanism cause both spatial and temporal correlations.

As the laser scanner's laser beam is send through the surrounding space (Figure 2), atmospheric conditions affect the stochastic characteristics of the distance measurements. Accordingly, temperature, atmospheric pressure and humidity have to be taken into account as correlating sources [31]. These factors change with time and space.

The object interacts directly with the laser beam and, hence, impacts the spatial correlations between the measured distances. A white object color, for example, leads to systematically longer measured distances compared to a black one [25]. Also the reflection, shape, roughness and entering depth, which are mostly all related to the object material, are factors for systematic influences on the observations [31].

The last listed cause for correlations in laser scanning is the scanning geometry. Primary, the distances and incidence angles depend on the position of the instrument related to the object. Both affect the random and systematic errors in the distance measurements and hence cause spatial correlations [24]. Narrow angles and long distances lead to overlapping footprints of the laser beam and, consequently, same information in neighbored points [31].

Summarizing, correlations at laser scanning are due to spatial as well as temporal effects and affect both angle as well as distance measurements. Herein, the spatial correlations of the distance measurements can be assumed to be of most relevance for deformation analyses [6], since most of the previously listed factors influence and correlate the distance measurements, not the angle measurements. Hence, spatial correlations of the distance measurement are analyzed in the present study. In prospective studies, the angle measurements should also be considered.

A measurement scene is schematically presented in Figure 2. The true shape of the object denotes the deterministic trend (functional model) in the measured point cloud. The functional model is usually expressed through a mathematical function [4, 15] which requires the knowledge of the surface's shape [31, 26].

If the trend is known, the measurements can be reduced by it. The remaining result consists of the stochastic signal and a random noise. These two components define the variances and covariances and, thus, the stochastic model. The stochastic signal includes all mentioned correlating effects and is defined as the colored noise. The random noise consists of all non correlating effects and is described as white noise. Yet, there is no common approach in seperating those components in real measurements (Section 2.3).

## 2.2 Preliminary investigations

TLS are still compulsory treated as 'black boxes' [32], since the exact construction and internal software corrections are not known in detail to the operator. Hence, there are many difficulties in detecting and handling correlations in laser scans and this task has not yet been solved. Contrary, for GNSS, methods for detecting and integrating correlations in the data processing exist due to a more profound knowledge about the relevant aspects (colored noise/autocorrelation in GPS, [18, 16]).

Following Schwieger (1999) [33], Kauker et al. (2016) compute an elementary error model of the scanned points [30]. Every spatiotemporal influence on a measured point is described as either a functional correlating, stochastic correlating or non-correlating error. All these errors are quantified based on assumptions and used to generate a synthetic covariance matrix [29]. This covariance matrix is applied in a simulation. Variances and correlations are calculated. The results detect high spatial correlations between the measured points.

Another approach is applied by Koch (2008) [23]. He repeatedly measured a wooden panel with a low resolution so that less than 50 points are generated on it. He collates the scans as time series of the measured points. The average 3D position of each point is subtracted as the trend of a function (as shown in Figure 2). The resulting residuals are used to calculate empirical auto covariance functions. This leads to a detection of high temporal correlations between the point coordinates. It has to be kept in mind that the definition of the detected correlations is not covering all effects mentioned in Section 2. While performing repeated measurements, some unchanged systematic effects might not be taken into account.

Consequently, all mentioned studies focus either on quantifying the theoretical effect of each correlation source on the correlation of measured scan points or aim at empirically revealing correlations. Nevertheless, the knowledge about correlations at laser scanning is still limited. Contrary to these previous studies, the present one investigates how much a parameter estimation is degraded due to this limited knowledge about correlations. The corresponding results can help at assessing the relevance of actually quantifying correlations at laser scanning in future studies.

## 2.3 Building of a more realistic stochastic model

Analyzing the data in terms of deformations and other high precision applications requires a correct functional and stochastic model in the appropriate adjustment to describe the measured situation in a sufficient way. Using a simulation approach allows an exact model definition. Nevertheless, the difficulties in devising these models for measured point clouds are explained in the following.

As written in Section 2.1, the stochastic model is defined by the variances and covariances of the measurements and, though, the covariance matrix $\mathbf{\Sigma}_{ll}$ (eq. 1). If correlations are not known, the covariance matrix equals a diagonal matrix:

$$\mathbf{\Sigma}_{ll} = \begin{pmatrix} \sigma_{s_1}^2 & 0 & 0 & 0 & \dots \\ 0 & \sigma_{\beta_1}^2 & 0 & 0 & \dots \\ 0 & 0 & \sigma_{t_1}^2 & 0 & \dots \\ 0 & 0 & 0 & \sigma_{s_2}^2 & \dots \\ \vdots & \vdots & \vdots & \vdots & \ddots \end{pmatrix}. \quad (1)$$

Here, $\sigma_{s_i}^2$, $\sigma_{\beta_i}^2$ and $\sigma_{t_i}^2$ denote the variance of the polar measurements distance $s$, vertical angle $\beta$, and horizontal direction $t$ of a point $i$. If no correlations are integrated in the covariance matrix, only a white noise is assumed [18]. However, correlations do exist in laser scans (Section 2.1) and, hence, colored noise has to be taken into account. Accordingly, the variances in eq. (1) are defined as follows, where the variance of the distance measurement is used exemplarily:

$$\sigma_{s_i}^2 = \sigma_{c_{si}}^2 + \sigma_{w_{si}}^2. \quad (2)$$

Here, the proportion of the variance regarding the colored noise is calculated as $\sigma_{c_{si}}^2 = r_c \cdot \sigma_{s_i}^2$. Equally, the proportion regarding the white noise can be calculated: $\sigma_{w_{si}}^2 = r_w \cdot \sigma_{s_i}^2$. Hence, every variance consists of a ratio of white $r_w$ and colored noise $r_c$, while their sum equals $r_w + r_c = 1$. Consequently, for calculating the covariances between two observations, the correlation coefficient has to be used [35]

$$\rho_{s_{i,j}} = \frac{\sigma_{s_{i,j}}}{\sigma_{c_{si}} \cdot \sigma_{c_{sj}}}, \quad (3)$$

which, in general, describes the stochastic dependencies between two random values $l_i$, $l_j$. Equivalent, the covariance $\sigma_{s_{i,j}}$ can be calculated when the other factors of eq. (3) are known. Finally, the covariance matrix in eq. (1) can be rewritten as:

$$\mathbf{\Sigma}_{ll} = \begin{pmatrix} \sigma_{s_1}^2 & 0 & 0 & \rho\sigma_{c_{s1}}\sigma_{c_{s2}} & \dots \\ 0 & \sigma_{\beta_1}^2 & 0 & 0 & \dots \\ 0 & 0 & \sigma_{t_1}^2 & 0 & \dots \\ \rho\sigma_{c_{s1}}\sigma_{c_{s2}} & 0 & 0 & \sigma_{s_2}^2 & \dots \\ \vdots & \vdots & \vdots & \vdots & \ddots \end{pmatrix}. \quad (4)$$

This matrix shows the correlation between two neighbored points regarding the distance measurements.

Consequently, for building a realistic covariance matrix, several aspects have to be known: the ratio of white noise $r_w$, the ratio of colored noise $r_c$, both leading to the level of complete noise, as well as the correlation coefficient between the observations $\rho$. While this has only been shown for the distance measurement's here, it might also be relevant for the angle measurements.

# 3 Simulating and evaluating correlations in laser scans

As written in Section 2, the exact magnitude and functional shape of correlations are unknown. Hence, for the simulation of correlated observations, certain assumptions have to be suggested. First, a description of the correlation function is needed which defines the correlation between two measured points on the object. In the next step, these correlations have to be integrated in the stochastic model where covariances can be calculated. Last, the generated covariance matrix can be used to add the stochastic information to simulated observations. This whole process is presented in Section 3.1 and 3.2.

The object used in this simulation is a $0.5 \times 0.5$ m plane. The distance between laser scanner and plane equals 10 m. The scan geometry is shown in Figure 3 where the red dots denote the scan points. The adjustment of the point cloud is explained in Section 3.3.

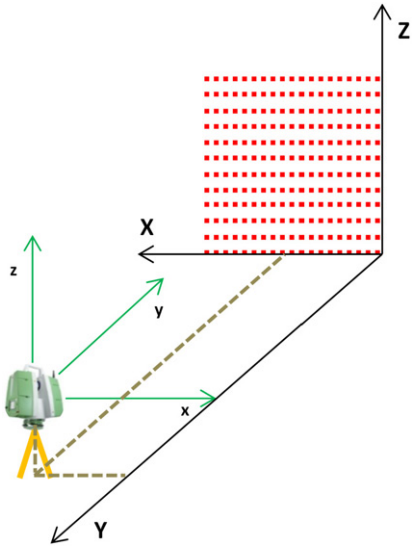


**Figure 3:** Scan geometry of the simulated scanning scene. The X, Y and Z axis define the object coordinate system (black). The x, y and z axis define the laser scanner coordinate system (green).

For analyzing the consistency and unbiasedness, Section 3.4 presents the statistical tests in terms of the sensitivity analysis (Section 1) which are used to evaluate the result of the parameter estimation.

## 3.1 Simulating correlation coefficients

In this study, correlations are assumed to decrease with an increasing distance between the points on the object.

This assumption is reasonable considering Section 2.1. To describe this behavior a quadratic exponential function is used [1]. Thus, the correlation function is defined as

$$\mathbf{R}_{i,j} = \exp\left(-\left(\frac{\mathbf{D}_{i,j}}{k}\right)^2\right). \tag{5}$$

$\mathbf{R}_{i,j}$ denotes the correlation between the point $i$ and $j$ and is equal to the defined correlation coefficient $\rho$ (eq. 3). The distance $\mathbf{D}_{i,j}$ between each of these points on the object is known, while the correlation length $k$ has to be defined. This factor determines the correlation's decrease. Figure 4 shows possible correlation functions with different correlation lengths $k$.

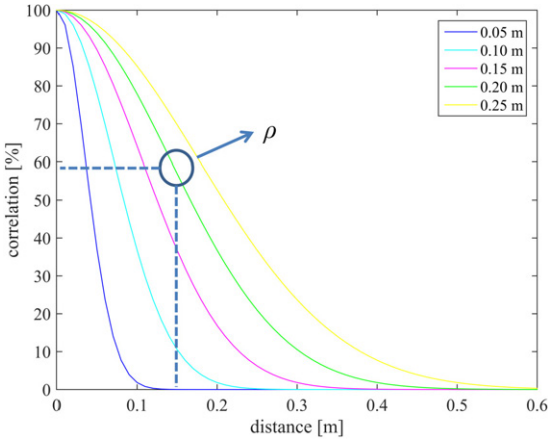


**Figure 4:** Quadratic exponential function (eq. 5) with different correlations lengths $k$ to describe the correlations in a simulated laser scan. The correlation coefficient $\rho$ can be picked out of the function.

The correlation length $k$ is defined as the distance between two points at which eq. (5) equals $\exp(-1) \approx 37\%$. That means if the distance between two points is smaller than the correlation length, the correlation is larger than 37%.

In reality, the correlation length is not known, furthermore one does not know whether eq. (5) describes all physical influences of correlations. Also, other possible correlation functions do not assign the causes of correlations to certain systematic effects yet (Section 2.1). To characterize the correlations, a list of various functions, e.g., linear exponential functions or radial basic functions, exist in literature [1, 9]. Here, a quadratic exponential function is chosen as initial guess. The general outcome of the study is unaffected by the assumed function. The effect of different functions describing correlations could be investigated in a proper study. In general, the correlation function should decrease exponentially with the distance between two points on the object based on the influencing sources named in Section 2.1.

Like mentioned, the stochastic model is usually a diagonal matrix due to unknown correlations (eq. 1). However, if the correlation function is known as in this simulation, covariances can be calculated.

In Figure 4, the approach to define the correlation coefficients $\rho$ is shown exemplarily for the correlation function with a correlation length of $k = 0.2$ m (green). Here, two points being approximately 15 cm apart from each other are correlated by $\rho \approx 58\%$. Directly neighbored points would be correlated with even more than 90%. Regarding eq. (3), these values are integrated in the stochastic model and, thus, used to calculate the covariances. Following, every entry is filled, so that the whole given stochastic information is integrated in the covariance matrix (eq. 4).

It can be seen that the spatial correlations are only integrated between the distance observations as described in Section 2.3. As a result, the covariances are known and the stochastic model can be generated as in eq. (4).

## 3.2 Correlating scan points

Calculating the covariances with regard to the ratio of colored noise is defined in eq. (2). This stochastic information is added to noise free observations to generate correlated observations. Therefore, the cholesky factorization is used. The cholesky factorization of a positive definite matrix is defined as [22]

$$\mathbf{\Sigma}_{ll} = \mathbf{Z}\mathbf{Z}^T, \tag{6}$$

where $\mathbf{Z}$ denotes a regular lower triangular matrix [21]. The transformation we are looking for is obtained through

$$\mathbf{l}_C = \mathbf{l}_G + \mathbf{Z} \cdot \boldsymbol{\epsilon}, \tag{7}$$

with $\boldsymbol{\epsilon} \sim \mathcal{N}(\mathbf{0}, \mathbf{I})$, a standard normal distributed vector, which is created randomly. $\mathbf{I}$ denotes the identity matrix. $\mathbf{l}_G$ defines the noise free observations and is marked by a $G$ due to the geometrical generating process. Now, the correlated observations $\mathbf{l}_C$ include the stochastic information since their distribution is $\mathbf{l}_C \sim \mathcal{N}(\mathbf{l}_G, \mathbf{\Sigma}_{ll})$.

As seen in Figure 1, different realizations of $\boldsymbol{\epsilon}$ considering the same correlation length lead to completely different systematic errors. In Section 2.1, the formative influence of correlations was explained. Now, the plotted points can be indicated as the product $\mathbf{Z} \cdot \boldsymbol{\epsilon}$, which can be specified as correlated residuals. The resulting impacts on parameter estimations will be quantified in Sections 4 and 5.

In Figure 5, two different correlation functions for a correlation length of $k = 0.05$ m and $k = 0.20$ m are illustrated. It shows how one point in the middle of the scanned plane is correlated to the other approx. 900 points on the surface. To define a characteristic variable which describes the strength of correlation in the point cloud of the scan, $n_c$ is defined. It denotes the number of points being correlated with more than $\rho > 37\%$ (see Section 3.1) to a point in the middle of the plane $n_{>37\%}$ (points lying above the red circle in Figure 5), compared to the number of all points $n_{all}$. Hence, $n_c$ is described as the rate of correlated points $n_c = n_{>37\%}/n_{all}$. This ratio does not change due to a changing point density.

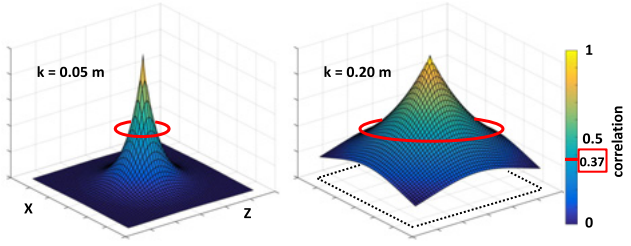


**Figure 5:** 3D correlation function of the simulated plane for a correlation length of $k = 0.05$ m and 0.20 m. Points which lies above the red circle are correlated with more than exp(−1) = 37% to the point in the middle of the function.

In Figure 5 left, $n_c$ is approx. 5%. Compared to Figure 5 right, this denotes a low impact of correlations, since the rate of correlated points is more than 54% here.

## 3.3 Plane approximation of the scan points

After simulating the correlated point cloud, a parameter estimation can be applied. The plane approximation is realized through a Gauss-Helmert model with a reduction to a Gauss-Markov model [13]. All the equations and descriptions for applying such an adjustment are presented in [8].

The used variances are taken from the Leica ScanStation P20 Laser Scanner accuracies [17]. The standard deviations of the distance is defined as $\sigma_s = 2$ mm, while angle measurements have a standard deviation of $\sigma_t = \sigma_t = 2.5$ mgon.

The functional model of a plane in the three-dimensional space is defined through

$$n_x \cdot x + n_y \cdot y + n_z \cdot z = d. \tag{8}$$

It is described by 4 parameters [28]. The estimated parameters $\hat{\mathbf{p}}$ consist of the normal vector $[\hat{n}_x, \hat{n}_y, \hat{n}_z]^T$ and the distance $d$ to the coordinate system's origin. The Cartesian coordinates $x = s\sin(\beta)\cos(t)$, $y = s\sin(\beta)\sin(t)$ and $z = s\cos(\beta)$ of one point are calculated based on the observation triplet $s, \beta, t$. Thus, all observed points $n$ consist of 3 observations each, which leads to a total of $m = n \cdot 3$ observations [8]. The redundancy accordingly equals $f = m - u$.

In the simulation, different point clouds can be generated. The correlation length $k$, the resolution of points on the object and the ratio of colored noise $r_c$ is modified. The influence on the parameter estimation of changing those factors is investigated in Sections 4 and 5.

## 3.4 Evaluating parameter estimates

To quantify the effect of unknown correlations in a parameter estimation of the plane, the results have to be analyzed. To evaluate the results following a sensitivity analysis [34], two statistical tests are formulated: the global test (Section 3.4.1) and the parameter test (Section 3.4.2). The global test is used to investigate the consistency of the adjustment, the parameter test investigates the unbiasedness. In general, a statistical test proves if an estimated value complies with a theoretical value, regarding a significance level $1 - \alpha$, where $\alpha$ denotes the error probability [35]. If it not complies, the test is rejected. Here, $\alpha$ is set to 1 %. Furthermore, it is shown how the estimated parameters are investigated regarding the true parameters which are known due to the simulation (Section 3.4.3).

### 3.4.1 Global test

A rejection of the global test is caused by either a wrong variance factor (see Section 3.4), functional model (eq. 8) or stochastic model $\mathbf{\Sigma}_{ll}$ (eq. 4). Since the investigations are implemented in a simulation, the variance factor and the functional model are exactly known. Consequently, a rejection of a test is ascribed to a false stochastic model (which is also known but is handled as unknown).

The test statistic $T_G$ for the global test is formulated as follows:

$$T_G = f \cdot \frac{\hat{s}^2}{\sigma_0^2} \sim \chi_f^2. \tag{9}$$

which is a $\chi_f^2$ distributed value. The empirical variance $\hat{s}^2$ is calculated by the resulting residuals $\hat{\mathbf{v}}$ and the matrix of weights $\mathbf{P}$ and is checked against the theoretical variance $\sigma_0^2$ (a-priori information) in consideration of $f$. With

$$\hat{s}^2 = \frac{\hat{\mathbf{v}}^T \mathbf{P} \hat{\mathbf{v}}}{f}, \tag{10}$$

and the relation between $\mathbf{P}$ and the cofactor matrix $\mathbf{Q}_{ll}$

$$\mathbf{\Sigma}_{ll} = \sigma_0^2 \mathbf{P}^{-1} = \sigma_0^2 \mathbf{Q}_{ll}, \tag{11}$$

the test statistic can be transformed into

$$T_G = \frac{\hat{\mathbf{v}}^T \mathbf{Q}_{ll}^{-1} \hat{\mathbf{v}}}{\sigma_0^2} = \hat{\mathbf{v}}^T \mathbf{\Sigma}_{ll}^{-1} \hat{\mathbf{v}}. \tag{12}$$

Here, the global test is formulated as a two sided test. This implicates calculating both quantile with half of the error probability $\frac{\alpha}{2}$:

$$\mathbf{P}\{\chi^2_{f,\alpha/2} \leq T_G \leq \chi^2_{f,1-\alpha/2}\} = 1 - \alpha. \tag{13}$$

For a better depiction of the results, the test statistic and the quantile are scaled by $f$,

$$\frac{T_G}{f} = \frac{\hat{\mathbf{v}}^T \mathbf{\Sigma}_{ll}^{-1} \hat{\mathbf{v}}}{f} \sim \mathcal{F}_{f,\infty}. \tag{14}$$

Since $f$ is the expectation value of an arbitrary $\chi^2_f$-distribution [35], values of around 1 are obtained. This is equal to a Fisher distribution with $f$ and $\infty$ as the two degrees of freedom.

Finally, eq. (13) can be formulated as

$$\mathbf{P}\left\{ \mathcal{F}_{f,\infty,\alpha/2} \leq \frac{T_G}{f} \leq \mathcal{F}_{f,\infty,1-\alpha/2} \right\} = 1 - \alpha. \tag{15}$$

#### 3.4.2 Parameter test

The test statistic $T_P$ proves the difference between the estimated parameters $\hat{\mathbf{p}}$ and their true values $\mathbf{p}$ considering the stochastic information from the covariance matrix of the estimated parameters $\mathbf{\Sigma}_{\hat{p}\hat{p}}$. Hence, the parameter test proves the unbiasedness of the parameter estimation:

$$T_P = \frac{1}{h}(\hat{\mathbf{p}} - \mathbf{p})^T \mathbf{\Sigma}_{\hat{\mathbf{p}}\hat{\mathbf{p}}}^{-1} (\hat{\mathbf{p}} - \mathbf{p}) \sim \mathcal{F}_{h,f}, \tag{16}$$

where $h$ denotes the number of parameters. $T_P$ is also Fisher distributed but tested one sided

$$T_P \leq \mathcal{F}_{h,f,1-\alpha}. \tag{17}$$

A rejection denotes that the difference between estimated and expected parameters is significant [27, 8]. This test formulation can be used in a simulation thanks to the knowledge of the true objects parameters $\mathbf{p}$.

#### 3.4.3 Estimated parameters and their covariance matrix

The parameter test only provides the decision of acceptance. As part of this test $\hat{\mathbf{p}} - \mathbf{p}$ and $\mathbf{\Sigma}_{\hat{p}\hat{p}}$ are calculated. To get a more detailed view, the change of those two components is analyzed separately in Section 5.2.

As the expressiveness of the dimensionless normal vector is limited, it is transformed to a vertical $\hat{\Theta}$ and horizontal angle $\hat{\Phi}$ indicating the orientation of the estimated plane:

$$\hat{\Theta} = \arccos\left( \frac{\hat{n}_z}{\sqrt{\hat{n}_x^2 + \hat{n}_y^2 + \hat{n}_z^2}} \right) \tag{18}$$

$$\hat{\Phi} = \arctan\left( \frac{\hat{n}_y}{\hat{n}_x} \right). \tag{19}$$

The variance propagation of this transformation has to be taken into account [8]. The new parameter vector $\hat{\mathbf{p}}_a = [\hat{\Theta}, \hat{\Phi}, d]^T$ and covariance matrix $\mathbf{\Sigma}_{\hat{p}_a\hat{p}_a}$ are obtained and used in Section 5.2

# 4 Impact of correlations on the consistence of the parameter estimation

As described in Section 2.3, the stochastic model in this simulation is not modeled correctly, since $\mathbf{\Sigma}_{ll}$ is a diagonal matrix (eq. 1). Consequently, this leads to an inconsistency of the adjustment which reflects the situation in the reality. Thus, it has to be investigated, whether one would notice the inconsistent modeling. Hence, the objective in this section is to analyze, how the correlations between the scanned points have to be increased until the global test detects an inconsistent stochastic model (Section 3.4.1).

As the way to generate correlated observations and evaluate the results is provided (Section 3), different simulated scenarios can be investigated. In further consequence, three factors are analyzed: the correlation length (Section 4.2), the spatial resolution on the object (Section 4.3) and the ratio of colored noise (Section 4.4). For each investigation one factor is changed, while the others stay the same. In general, 995 points are generated, whereby the lowest distance between two points is at least 1.58 cm. The ratio of colored noise is assumed to be $r_c$ = 70%.

The scan geometry and the scanned object stays the same. That means the TLS scans a 0.5 m × 0.5 m plane in a distance of 10 m. The variances of the measurements are defined in Section 3.4.

## 4.1 Knowledge about correlations

Figure 1 already showed that correlations have a formative effect. If there were no correlations in laser scans, the re-

sulting residuals of a plane approximation would appear as random noise as it can be seen on the left side of Figure 6. The effect of increasing the correlation length gradually is also shown.

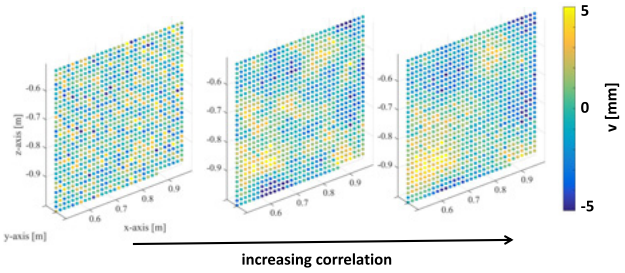


**Figure 6:** Increasing the correlation length in the observations.

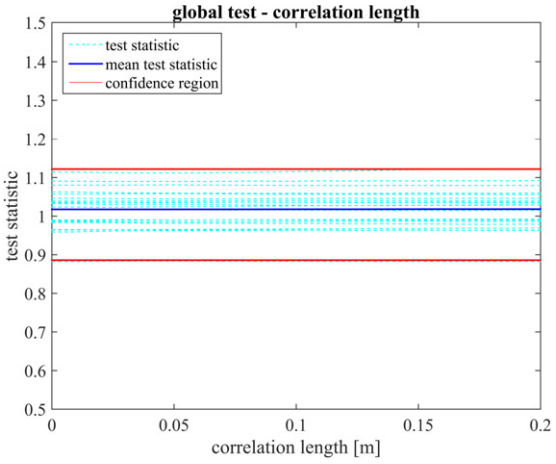


**Figure 7:** Implementation of the global test for the first case while increasing the correlations.

The higher the correlations, the more systematic the residuals, concerning their magnitude and direction. Thus, the correlation length determines the areal extent of the systematic influence on the residuals. Therefore, the following investigations all contain the increase of the correlation length. Hence, Figure 6 shows the generated observations in a descriptive way.

## 4.2 Correlation length

In this simulation, two cases are investigated:

1. The observations are correlated according to Section 3. The covariance matrix is filled with the corresponding covariances. This is the theoretical case for validating the results.
2. The observations are correlated according to Section 3. However, the covariance matrix is a diagonal matrix (eq. 1). This corresponds to the real situation, since it is assumed that there is no knowledge about the existing correlations (Section 2). This case is of a higher interest here.

For both cases, the global test is implemented with the settings according to the begin of this section, while increasing the correlation length for the observations. Figure 7 shows the results of the first case.

Here, every light blue line denotes the test statistic of one realization of the standard normal distributed vector $\boldsymbol{\epsilon}$ (eq. 7). In terms of reducing the random variations, the mean test statistic is marked by the blue line and calculated as the average of 100 realizations (20 are shown). The confidence region is defined by the two red lines. It is constant due to the constant number of points (see eq. 15).

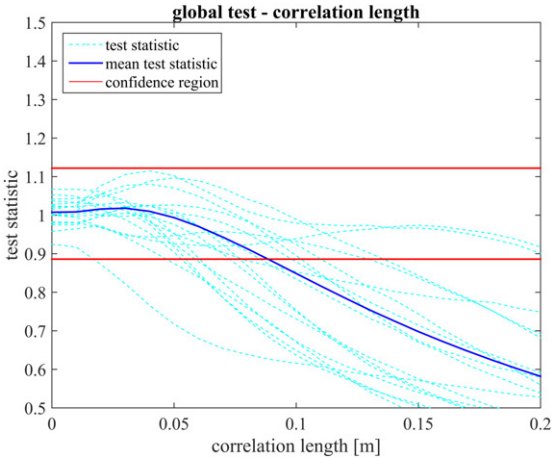


**Figure 8:** Implementation of the global test for the second case while increasing the correlations.

The correlation length (eq. 5) is increased in steps of $\delta k = 0.01$ m until $k = 0.2$ m is reached. The generated observations change successively as shown in Figure 6.

The test statistics show small differences, however they have a similar functional behavior. As can be seen for the mean statistic, the test is accepted even if the correlation is set the highest. Hence, the global test attests a correct stochastic model in the adjustment. This consistent modeling was expected, since the covariance matrix $\Sigma_{ll}$ considered the covariances. Thus, if the correlations were known, the adjustment would be consistent.

This setup is also performed for the second case where the correlations are handled as unknown (Figure 8).

Here, a different result occurs. The single test statistics (light blue) are rejected at a correlation length from

$k = 0.02$ m to $k > 0.20$ m. They vary due to the random process. The mean test statistic is getting smaller while increasing the correlation length. It is rejected at approx. $k = 0.08$ m. This entails the effect of neglecting correlations in the stochastic model: the global test is rejected at a certain point of correlation length. This denotes an inconsistent modeling.

## 4.3 Spatial resolution

The next investigations are performed for the second case regarding different settings to see how the level of rejection differs. Since increasing the correlation length leads to a rejection of the global test, the resolution as another factor is considered. Therefore, the same setup as in Figure 8 is applied for different numbers of scanned points. The varying resolutions sequentially lead to 25, 49, 100, 225 and 995 points on the object (Figure 9). For a better overview, only each mean test statistic (out of 100 realizations) is plotted.

The functions of the test statistics do not distinguish much. However, the confidence region changes due to the changing redundancy $f$ (see eq. 15). This is represented by the red dotted line for 25 scan points and by the red normal line for 995 points (Figure 9). The other boundaries lie between these lines.

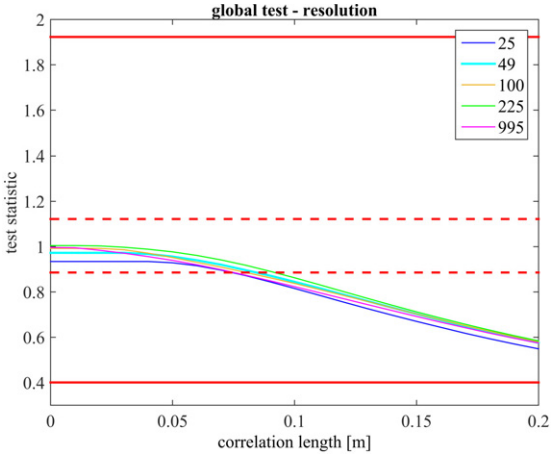


**Figure 9:** Global test for different number of scanned points due to the change of resolution.

Accordingly, a higher object resolution leads to an earlier rejection of the global test. Table 1 denotes the value of correlation length at which the respective test statistic is rejected. Also the related rate of correlated points $n_c$ (Section 2.1) as well as the point spacing between two neighbored points is presented.

**Table 1:** Global test: Parameter estimation for a different number of points which are respectively rejected at different correlation lengths $k$. Also the ratio of correlated points $n_c$ and the point spacing are plotted.

| numb. of points | $k$ at rejection | $n_c$ | point spacing |
|---|---|---|---|
| 25 | > 20 cm | 49 % | 8.97 cm |
| 49 | > 20 cm | 49 % | 6.63 cm |
| 100 | 16.3 cm | 31 % | 4.75 cm |
| 225 | 11.9 cm | 17 % | 3.21 cm |
| 995 | 7.5 cm | 7 % | 1.58 cm |

The rejection for a resolution of 25 or 49 points on the object cannot be seen in this Figure 9. It will be rejected at a higher correlation length of approx. $k = 0.25$ m. Thus, it needs a rate of more than 49 % of correlated points until the global test is rejected. For 995 points, already a small correlation length of 7.5 cm detects a false stochastic model. According to a smaller point spacing of 1.58 cm, systematic effects cause a higher correlation between the scanned points. Thus, already a rate of 7 % of correlated points on the scanned plane leads to an inconsistent modeling.

Consequently, a higher resolution leads to a more distinct detection of the inconsistency due to a smaller confidence region in the global test (eq. 15).

## 4.4 Ratio between colored and white noise

Until now, the ratio of colored noise $r_c$ (eq. 2) was set to 70 %. Now, the ratio changed while using a constant resolution of 995 points. If $r_c$ is set higher, correlating effects have a stronger influence on the variances than the random effects (eq. 2). Moreover, the covariances will get larger, since the correlations are positive.

In Figure 10, the global test shows the change of the test statistic due to different $r_c$ (15 %, 30 %, 45 %, 60 %, 75 %). The confidence region stays the same for every setting because the resolution is fixed (eq. 15). It can be seen that the higher the rate of colored noise, the earlier the global test is rejected. This is an expected result since the covariances increase according to eq. (2).

Table 2 shows the correlation length at which the test is rejected. The number of points on the object stays the same. Thus, for a higher ratio of colored noise (more than 45 %), a small ratio of correlated points ($n_c < 10$ %) leads to a distinct rejection of the test. Hence, setting the ratio of colored noise $r_c$ higher leads to an earlier detection of the inconsistent stochastic model. It has to be kept in mind that the correlations will not change while increasing $r_c$.

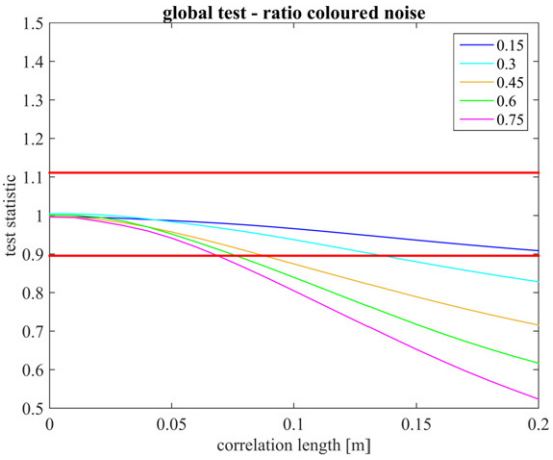


**Figure 10:** Global test for different ratios of colored noise $r_c$ (eq. 2).

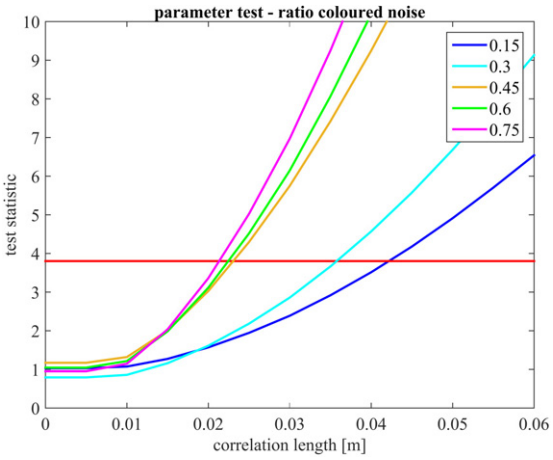


**Figure 11:** Parameter test for different ratios of colored noise $r_c$ (eq. 2).

**Table 2:** Parameter test: Parameter estimation for a different ratio of colored noise which are respectively rejected at different correlation lengths $k$. Also the ratio of correlated points $n_c$ is plotted.

| ratio $r_c$ | $k$ at rejection | $n_c$ |
|---|---|---|
| 0.15 | > 20 cm | 49 % |
| 0.30 | 13.6 cm | 23 % |
| 0.45 | 8.8 cm | 9 % |
| 0.60 | 7.6 cm | 7 % |
| 0.75 | 6.9 cm | 6 % |

However, the covariances increase as it can be seen in eq. (2). Thus, knowing the true value of colored to white noise is important to know for assessing the impact of correlations.

# 5 Impact of correlations on the unbiasedness of the parameter estimation

Using the global test enables detecting the inconsistent stochastic model in the parameter estimation. Besides, the estimated parameters $\hat{\mathbf{p}}$ and their covariance matrix $\mathbf{\Sigma}_{\hat{p}\hat{p}}$ can be investigated. Now, since the expected values $\mathbf{p}$ of the plane are indeed known in the simulation, a validation in terms of unbiasedness can be implemented. Sections 5.1 and 5.2 show the results.

## 5.1 Results of the parameter test

Using the parameter test leads to similar conclusions as the global test does when regarding the correlation length, resolution and ratio of colored noise (Sections 4.2–4.4). But in difference to these previous results, the parameter test is declined already for shorter correlation lengths $k$. Figure 11 shows the results for different ratios of colored noise analogous to Figure 10 for the global test. If a test statistic lies above the red line, the one sided parameter test is rejected (eq. 17). Here, the horizontal axis is scaled compared to Figure 10 to focus on the correlation lengths at which the test is declined. With the parameter test, the wrong stochastic model can already be detected at about a quarter of the correlation length at which the global test is declined.

## 5.2 Estimated parameters and covariance matrix

To investigate the absolute change of estimated parameters, the vertical angle $\hat{\Theta}$, horizontal angle $\hat{\Phi}$ (eq. 18, 19) and the distance $\hat{d}$ are examined separately.

In Figure 12, the known correlations are not implemented in $\mathbf{\Sigma}_{ll}$ (second case of Section 4.2). This is simulated with the same settings as presented in Section 4 (995 scan points, $r_c = 70\,\%$). Here, the resolution and the ratio of colored noise are fixed. Figure 12 shows the difference between estimated parameters and true values: $|\hat{\mathbf{p}} - \mathbf{p}|$. The $3\hat{\sigma}$ level of the estimated parameters is plotted and used to highlight the significance of these differences. The correlations between the estimated parameters are neglected by this.

As the correlation length increases, the estimated parameter values change. In contrast to the parameter estimates, the standard deviations are unaffected from the increasing correlation. This is due to the fact that the known

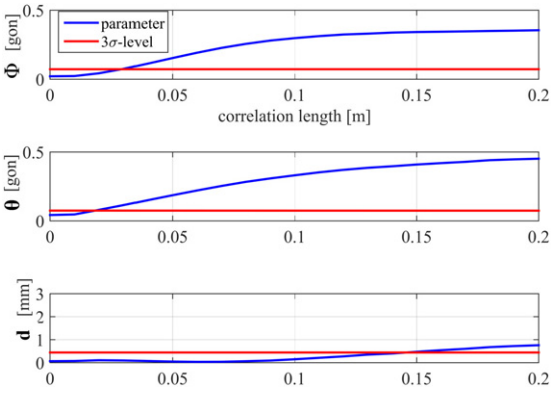


**Figure 12:** Difference of estimated parameters due to the true values for the implementation of the second case.

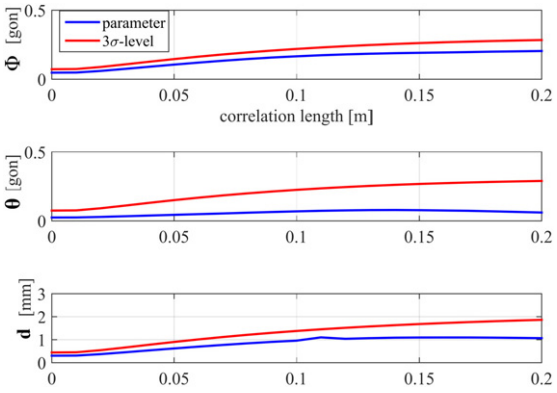


**Figure 13:** Estimated parameters of the plane for the implementation of the first case.

correlations are not integrated in the stochastic model here. These certainties lead to the decline of the parameter test with increasing correlation length.

For comparison, the covariance matrix of the observations is now additionally filled with the known correlations (first case of Section 4.2). The resulting parameter estimates and their $3\hat{\sigma}$ are shown in Figure 13 similar to Figure 12.

On the one hand, the true stochastic model leads to less biased parameter estimates compared to Figure 12. On the other hand, the estimated standard deviations now depend on the correlation length. This time, these certainties lead to the acceptance of the parameter test independent from the correlation length.

Consequently, the parameter estimates are unbiased and the estimated parameter precision is more realistic if the correlations were known.

# 6 Discussion

The previous sections provide the impact of neglecting correlations in a parameter estimation of a laser scan. In Section 4, the inconsistency of the stochastic model is indicated due to the rejection of the global test (Figure 4). Section 5 shows the resulting bias in the estimated parameters. Here, the parameter test indicates a significant difference between the estimated and the expected values (Figure 11).

These results are already obtained considering relatively low correlations. As seen in Figure 5, a correlation length of $k = 0.05$ m causes a 5 % ratio of correlated points (Section 3.2). Sections 5.1 and 4.2 state that this areal extent of correlations already causes an impact on the consistence and unbiasedness of the parameter estimation regarding the simulated number of points and ratio of colored noise.

The comparison between global test (consistency) and parameter test (bias) reveals one further important outcome: Even at short correlation lengths, the parameters are estimated biasedly – indicated by a declined parameter test. At the same time, the consistence of the adjustment is still given – indicated by an accepted global test. In real applications, only the global test can be performed since the true parameters are not known. Hence, the accepted global test might indicate in these cases that the estimation is successful, although the estimated parameters are indeed biased concerning the used stochastic model that neglects correlations.

As to capture the mentioned application of a deformation analysis (Section 2.1), the given statements above point out critical issues. Since the correlations have a formative effect on the scanned point cloud (Figure 1), results in high precision approaches might not be able to distinguish between deformations and correlations. Thus, neglecting correlations leads to an inconsistent estimation of deformation parameters and their covariance information. Furthermore, the estimated parameters might appear to be biased. A statistical analysis of the deformation following [27] is not applicable in this case.

Finally resumed, if the unknown correlation in laser scan measurements were known the parameter estimation would improve:

- the estimated parameters would be unbiased
- the estimated covariance matrix of the parameters would be more realistic.

Both points combined lead to a deformation analysis that would allow for a detection of even small parameter changes between two epochs.

# 7 Conclusion and outlook

This study investigates the impact of unknown correlations in laser scans on the results of a parameter estimation in terms of a sensitivity analysis as written in [34]. Therefore, several point clouds of a plane are simulated which vary in the correlation length, the ratio of colored noise and the number of points. The higher the values of these factors are, the more increases the covariance between the scanned points. An adjustment is implemented to estimate the object parameters and it's covariance matrix and to reveal the impact of the correlations on these estimations. Statistical analysis is used to evaluate the results.

If the correlation length is increased, the global test is declined at some point indicating an inconsistent stochastic model. A similar behavior is achieved using the parameter test indicating biased parameter estimates. Of importance is that the parameter test – that can only be used if the true parameters are known – is declined already with shorter correlation lengths than the global test. This means: Even if the global test attests a parameter estimation to be successful, it might be biased due to unknown correlations. Therefore, the determination of correlations at laser scanning is an important task for laser scanner based deformation analyses or other applications with high demands regarding accuracy.

Hence, it is important to investigate the existing correlations in laser scans. In a further step, the empirical calculation of a covariance function could be examined. Kuhlmann (2001) [18] shows an improving effect in terms of statistical tests when using such an empirically covariance matrix in the adjustment of a GPS measurement. There are also other ways to yield statistical information. Kauker et al. (2016) [30] try to model the covariance matrix using empirical values and functional relations.

Therefore, a way to acquire correlations empirically has to be designed. This could be realized by reference objects whose geometries are known with superior accuracy to eliminate the trend in the observations as shown in Figure 2. In case of laser scanners, a measuring arm or laser tracker are able to provide point accuracies of better than 0.1 mm [19]. Measuring a large object could help to investigate and quantify the correlating effects of scanner and object characteristics, scan geometry and atmosphere while modifying these factors.

# References

[1] Ishimaru A., *Wave Propagation and Scattering in Random Media*, Wiley-IEEE Press, 1997.

[2] Pesci A., Teza G., Bonali E., Casula G. and Boschi E., A laser scanning-based method for fast estimation of seismic-induced building deformations, *ISPRS Journal of Photogrammetry and Remote Sensing* **79** (2013), 185–198.

[3] Harmening C., Kauker S., Neuner H. and Schwieger V., Terrestrial Laserscanning – Modeling of Correlations and Surface Deformations, *FIG Working Week 2016, Chirstchurch, New Zealand* (2016).

[4] Hesse C. and Kutterer H., Automated Form Recognition of Laser Scanned Deformable Objects, *Geodetic Deformation Monitoring: From Geophysical to Engineering Roles* **131** (2005), 103–111.

[5] Holst C., Nothnagel A., Blome M., Becker P., Eichborn M. and Kuhlmann H., Improved area-based deformation analysis of a radio telescopes main reflector based on terrestrial laser scanning, *Journal of Applied Geodesy* **9** (2014), 1–13.

[6] Holst C. and Kuhlmann H., Challenges and Present Fields of Action at Laser Scanner Based Deformation Analyses, *Journal of Applied Geodesy* **10** (2016), 17–25.

[7] Holst C., Neuner H., Wieser A., Wunderlich T. and Kuhlmann H., Calibration of Terrestrial Laser Scanner, *Allgemeine Vermessungs-Nachrichten* **6** (2016).

[8] Holst C., Artz T. and Kuhlmann H., Biased and unbiased estimates based on laser scans of surfaces with unknown deformations, *Journal of Applied Geodesy* **8** (2014), 169–183.

[9] Rasmussen C. and Williams C., *Gaussian Processes for Machine Learning*, MIT Press, Cambridge, 2006.

[10] Eling D., *Terrestrisches Laserscanning für die Bauwerksüberwachung*, Ph.D. thesis, Leibniz Universität Hannover, 2009.

[11] Lichti D., Stewart M., Tsakiri M. and Snow J., Calibration and testing of a terrestrial laser scanner, *International Archives of Photogrammetry and Remote Sensing* **XXXIII** (2000).

[12] Schneider D. and Maas H.-G., Integrated bundle adjustment with varicance component estimation – fusion of terrestrial laser scanner data, panoramic and central perspective image data, *ISPRS Workshop on Laser Scanning* (2007).

[13] Mikhail E. and Ackermann F., *Observations and least squares*, Dun-Donelly, New York, 1976.

[14] Serantoni E. and Wieser A., TLS-based Deformation Monitoring of Snow Structures, *Schriftenreihe des DVW Band 85, Terrestrisches Laserscanning* (2016).

[15] Kermarrec G. and Schön S., A priori fully populated covariance matrices in least squares adjustment – case study GPS: relative positioning, *Journal of Geodesy* (2016), 1–20.

[16] Kermarrec G. and Schön S., Taking correlations in GPS least squares adjustments into account with a diagonal covariance matrix, *Journal of Geodesy* **90** (2016), 793–805.

[17] Leica Geosystems, Leia ScanStation P20 – data sheet, *Leica Geosystems* (2013).

[18] Kuhlmann H., Importance of autocorrelation for parameter estimation in regression models, *10th FIG International Symposium on Deformation Measurements* (2001).

[19] Faro Technologies Inc., Faro Products – Portable systems for measurement and 3D documentation, (2012).

[20] Wang J., *Towards deformation monitoring with terrestrial laser scanning based on external calibration and feature matching methods*, Ph.D. thesis, Leibniz Universtität Hannover, 2013.

[21] Koch K.-R., *Parameter Estimation and Hypothesis Testing in Linear Models*, Springer, 1999.

[22] Koch K.-R., *Introduction to Bayesian Statistics*, Springer, 2007.
[23] Koch K.-R., Determining uncertainties of correlated measurements by Monte Carlo simulations applied to laserscanning, *Journal of Applied Geodesy* **2** (2008).
[24] Zamecnikova M. and Neuner H., Untersuchung des gemeinsamen Einflusses des Auftreffwinkels und der Oberflächenrauheit auf die reflektorlose Distanzmessung beim Scanning, *Ingenieurvermessung* **17** (2017). Wichmann, Berlin, 63–76.
[25] Zamecnikova M., Neuner H. and Pegritz S., Influence of the Incidence Angle on the Reflectorless Distance Measurement in Close Range, *INGEO – 6th International Conference on Engineering Surveying, Prague* (2014).
[26] Zamecnikova M., Neuner H., Pegritz S. and Sonnleitner R., Investigation on the influence of the incidence angle on the reflectorless distance measurement of a terrestrial laser scanner, *Vermessung und Geoinformation* **2+3** (2015), 208–218.
[27] Heunecke O., Kuhlmann H., Welsch W., Eichhorn A. and Neuner H., *Auswertung geodätischer Überwachungsmessungen, Handbuch Ingenieurgeodäsie*, (Moser M., Müller G. & Schlemmer H.), Heidelberg: Wichmann, 2. ed., 2013.
[28] M. Peternell, Developable surface fitting to point clouds, *Comput. Aided Geom. D.* **21** (2004), 785–803.
[29] Kauker S., Holst C., Schwieger V., Kuhlmann H. and Schön S., Spatio-temporal Correlations of Terrestrial Laser Scanning, *Allgemeine Vermessungs-Nachrichten* **6** (2016), 170–182.
[30] Kauker S. and Schwieger V., First investigations for a synthetic covariance matrix for monitoring by terrestrial laser scanning, *Joint International Symposium on Deformation Monitoring* (2016).
[31] Soudarissanane S., Lindenbergh R., Menenti M. and Teunissen P., Scanning geometry: Influencing factor on the quality of terrestrial laser scanning points, *ISPRS Journal of Photogrammetry and Remote Sensing* **66** (2011), 389–399.
[32] Schulz T., *Calibration of a Terrestrial Laser Scanner for Engineering Geodesy*, Ph.D. thesis, Technical University of Berlin, 2007.
[33] Schwieger V., *Ein Elementarfehlermodell für GPS-Überwachungsmessungen – Konstruktion und Bedeutung interepochaler Korrelationen*, Ph.D. thesis, Vermessungswesen der Universität Hannover, 1999.
[34] Schwieger V., *Nicht-lineare Sensitivitätsanalyse gezeigt an Beispielen zu bewegten Objekten*, Habilitation, 2005.
[35] Niemeier W., *Ausgleichungsrechnung – Statistische Auswertemethoden*, Berlin, Walter de Gruyter, 2008.